Acta Geodyn. Geomater., Vol. 5, No. 4(152), 361–375, 2008

STRESS AND DEFORMATION STATES IN UNDERGROUND STRUCTURES USING COUPLED MODELLING

Petr PROCHÁZKA [1] and Jiřina TRČKOVÁ [2]*

[1] *Czech Technical University, Faculty of Civil Engineering, Thákurova 7, Prague 6, Czech Republic*
[2] *Institute of Rock Structure and Mechanics, Academy of Sciences of the Czech Republic, v.v.i., V Holešovičkách 41, 182 09 Prague , Czech Republic*
**Corresponding author's e-mail:* trckova@irsm.cas.cz

(*Received* July 2008*, accepted* October 2008)

ABSTRACT
The techniques of the method of the coupled modelling was substantially extended and used for solving problems connected with underground constructions for various materials and appropriate structural systems. In principle, a combination of linear effects of the external loading and material and time-dependent nonlinear change in structures was considered. Assessment of rock behaviour in surrounding of utility tunnels, solution of the structural strength below foundation, back analysis of reinforced soil slopes and studies of slopes endangered by groundwater were carried out.

KEYWORDS: physical and numerical modelling, rock behaviour, slopes, tunnels, inverse analysis

1. INTRODUCTION

Numerical methods seem to be the cheapest tool for assessing different types of structures. If the theory of damage should be involved into the formulation of the problem to be solved, special treatment is required. The experiments have been carried out to get knowledge about a reasonable approach for solving the problem. On the basis of the results from experiments based on the principles of physical modelling the development of constitutive equations for inelasticity and damage of heterogeneous materials that benefit from some specificities of a special boundary element method have been carried out. On one hand side, we need to obtain better approximations of the local stress and strain fields than in the standard approaches based on experience, especially when considering damage and failure conditions. It tends to simplify sufficiently the numerical techniques of overall homogenization in order to obtain a treatable system of equations that could recover the status of a constitutive equation.

Models are considered for application to plasticity, viscoelasticity and damage in soil/rock material. Model by (Kachanov, 1992) is mostly used. The method proposes a continuation and development of Desai's DSC which has formerly been used for saturated soils and then extended to solid materials. The extension by Desai consisted in inclusion of skeleton into the consideration and solution of such problems, which were coupled (mutual interaction of water and skeleton was studied). Procházka and Trčková (Procházka and Trčková, 2000) introduced previously piecewise uniform eigenstrains in each material phase and précised the properties of the phases. Standard applications of the method to a two-phases rock material (stone, clay) are considered in this study, it means only one sub-volume per phase is considered. A typical application of coupled modelling (experimental and numerical) to special case of patterns was published in (Trčková and Procházka, 2001; Trčková and Procházka, 2006).

This article summarized brief description of the numerical and experimental methods which have been applied to assessment of rock behaviour in surrounding of utility tunnels, solution of the structural strength below foundation and for back analysis of reinforced soil slopes in the frame solution of the grant project "Stress and deformation states in structures and structural elements using coupled modelling".

2. ASSESSMENT OF ROCK MASS BEHAVIOUR IN SURROUNDING OF UTILITY TUNNELS

The fundamental ideas of a numerical procedure leading to overall plastic and damage behaviour of rock matrix in a rock – tunnel lining aggregate is presented. Based on the numerical models and mechanical laws it is possible to obtain the strain and stress from results of experimental scale models. Very important property of the above procedure is the non-linearity of the problem, which, when using some smart algorithm, can be solved by very powerful iterative process.

Underground utility tunnels and other technological and specific tunnels constructed in small depths under the surface occur often under building foundations especially in an urban area. These tunnels and foundations of the ground structures can interact mutually and influence their stability and cause adverse reaction. Redistribution of the stress around

the tunnel depends not only on properties of environmental soils, and tunnel size and location, but also on tunnel lining stiffness (Jao and Wang, 2000). This study focuses on coupled modelling of this problem. On experimental and numerical models distribution of stress around horizontally located circular tunnel with diameter about 1.6 m under the strip footings in dependence on the lining stiffness was carried out. Experiments were performed on a scale of 1:20 in modelling stand. The analysis was focused on determining stress distributions due to construction of strip footing above existing tunnel lined by lining of various thicknesses.

On the basis of experiment results, internal parameters for numerical models were determined. In numerical models Desai´s Distinct State Concept (Desai, 1994) was combined with Transformation Field Analysis (Dvorak, 1992; Dvorak and Procházka, 1996). The procedure may be considered as a special case of inverse analysis.

2.1. NUMERICAL MODELLING

2.1.1. FORMULATION OF TFA

In this section, our aim is to formulate the general procedure for the TFA. This may be done in terms of many modern numerical methods. First, let us consider that the body (part of a structure, element, system of more elements, composite) behaves linearly; i.e. Hooke's linear law is valid in entire body (this assumption admits among others an application of the BEM). When the problem is correctly posed, the displacement vector, strain and stress tensors can be obtained from the Navier equations, kinematical equations, and the linear Hooke's law.

In the second step we select points, where the measured values are available, either from experiments in laboratory, or from "in situ" measurements. We also select points, or regions (subdomains) from the body under study, and apply there successively unit eigenparameter impulses (either eigenstresses or eigenstrains) to get an influence tensor (matrix). In order to precise this statement, denote A_i, $i = 1,...,n$, either the points or regions where the eigenparameters will be applied. Let, moreover, the set of points where the measured values are known be $B_j, j = 1,...,m$. Then the real stress at B_j is a linear hull of stress σ^{ext} at B_j due to external loading and eigenstrains μ and ε^{pl}, or eigenstress λ and relaxation stress σ^{rel} at A_i (similar relations are valid for overall strain field ε):

$$\sigma = \sigma^{ext} + P^{\sigma}\mu + Q^{\sigma}\varepsilon^{pl} \quad , \quad \text{or}$$

$$\sigma = \sigma^{ext} + R^{\sigma}\lambda + T^{\sigma}\sigma^{rel} \quad , \tag{1}$$

$$\varepsilon = \varepsilon^{ext} + P^{\varepsilon}\mu + Q^{\varepsilon}\varepsilon^{pl} \quad , \quad \text{or}$$

$$\varepsilon = \varepsilon^{ext} + R^{\varepsilon}\lambda + T^{\varepsilon}\sigma^{rel} \quad , \tag{2}$$

or in differential (incremental) form:

$$d\sigma = d\sigma^{ext} + P^{\sigma}d\mu + Q^{\sigma}d\varepsilon^{pl} \quad , \quad \text{or}$$

$$d\sigma = d\sigma^{ext} + R^{\sigma}d\lambda + T^{\sigma}d\sigma^{rel} \quad , \tag{3}$$

$$d\varepsilon = d\varepsilon^{ext} + P^{\varepsilon}d\mu + Q^{\varepsilon}d\varepsilon^{pl} \quad , \quad \text{or}$$

$$d\varepsilon = d\varepsilon^{ext} + R^{\varepsilon}d\lambda + T^{\varepsilon}d\sigma^{rel} \quad , \tag{4}$$

where the influence tensors P, Q, and R and T may be identical (in the case of the TFA they must be identical, as they describe generalized linear Hooke's law, and $\mu = \varepsilon^{pl}$, $\lambda = \sigma^{rel}$), as any eigenparameter may stand for the plastic or relaxation parameter (say, eigenstrain may stand for plastic strain, which is obvious from (1)). The dimensions of σ, σ^{ext}, μ, ε^{pl}, λ, and σ^{rel} are $m \times 6$ (because of symmetric stress and strain tensors) and the dimensions of P and Q are $m \times 6 \times n$. In the classical TFA the values of μ, or ε^{pl} are calculated from minimization of variance of computed and measured stresses. It holds: $\lambda = - C \mu$.

The first relations in (1) and (3) describe the initial strain method while the second relations in those equations formulate the initial stress method. The eigenparameters may generally stand for plenty of phenomena like change of temperature, swelling, watering, etc. This is why we could split the eigenparameters in (1) into two parts: eigenparameters themselves and the quantities connected with physically nonlinear behaviour of the material.

2.1.2. DISTURBED STATE CONCEPT (DSC)

The idea of this theory was originally proposed by Desai, and the theory characterized behaviour of over-consolidated clays. Since then, Desai and co-workers have developed and successfully applied this concept to other materials (Desai, 1994).

The DSC is a unified modelling theory for mechanical behaviour of material and interfaces. It allows incorporation of the internal changes on interfacial boundaries of phases (both micro- and macro level) and the resulting mechanism in a deforming material into the constitutive description. Initially, the material under external loading is in relative intact state (IS). Using such theories as elasticity, plasticity and viscoplasticity may theoretically treat the intact state, i.e. no cracking is considered in this state. After increasing the external loading, the material transforms from the IS state to the fully adjusted state (FA) or critical state, which is an asymptotic state, the material at that may no longer carry certain or all stresses. For example, micro cracking and subsequent softening are such disturbances.

Desai uses a scalar disturbance function D, having different expressions depending of mechanical properties in the model under consideration. The equilibrium equation for a material element in terms of stresses is derived as:

$$D_u S_{ij} = (D_u - D)s_{ij}^{IS} + Ds_{ij}^{FA} \quad , \tag{5}$$

where S_{ij} stands for average (observed) response, D_u is max D and is in most cases equal to one. Using

the incremental method, the differentiation of the last relation yields:

$$D_u dS_{ij} = (D_u - D) d\sigma_{ij}^{IS} + D d\sigma_{ij}^{FA} + dD(\sigma_{ij}^{FA} - \sigma_{ij}^{IS}) \quad (6)$$

The first term of the right hand side of the last equation expresses continuum constitutive law for elastic-plastic (visco-plastic) behaviour, the second term obeys the classical Kachanov damage formulation (Kachanov, 1992), and the third term in (6) indicates different stresses in the two parts.

The incremental constitutive equations for the IS part and the FA part are expressed as:

$$d\sigma_{ij}^{IS} = C_{ijkl}^{IS} \varepsilon_{kl}^{IS} \ , \quad d\sigma_{ij}^{FA} = C_{ijkl}^{FA} \varepsilon_{kl}^{FA} \ , \quad (7)$$

where C^{IS}_{ijkl} are in our case the components of von Mises-Huber-Hencky constitutive tensor IS part, furthermore C^{FA}_{ijkl} are the components of damage constitutive tensor for FA part, superscripts IS and FA indicate the phases. For more details concerning the DSC see Desai's publications cited in References.

For Hooke's law with Mises condition involving eigenstrain it holds in incremental form:

$$\varepsilon_{ij}(du) = A_{ijkl} d\sigma_{kl} + d(\varepsilon_{ij})^{pl} + \mu_{ij} \ , \quad (8)$$

where (Duvant and Lions, 1972):

$$(\varepsilon_{kl})^{pl} = 0 \quad \text{for} \quad F(\sigma) < 0 \quad \text{and}$$
$$(\varepsilon_{kl})^{pl} = 1/(2Gs)/(s-k)(\sigma_{ij})^D \quad \text{for} \quad F(\sigma) > 0,$$
$$2s^2 = (\sigma_{ij})^D (\sigma_{ij})^D \ ,$$

and $(\sigma_{ij})^D$ are components of deviatory part of the stress tensor, $F(\sigma)$ is the function of plasticity, which is defined for Mises model as:

$$F(\sigma_{ij}) = \tfrac{1}{2}(\sigma_{ij})^D (\sigma_{ij})^D - k^2 \ .$$

In the last formulas G is the shear modulus, k is a material positive constant.

Using the dual transformation formulated by Duvant and Lions, we arrive at the following variation principle:

$$\int_\Omega [\tfrac{1}{2}\kappa(divu)^2 + \Phi(\varepsilon^D)u] \, dx - \int_\Omega f_i u_i dx - \int_{\Gamma_p} p_i u_i dx \to \min \quad (9)$$

where

$$\Phi(\varepsilon^D) = G(\varepsilon_{ij})^D (\varepsilon_{ij})^D \quad \text{for} \quad 2G^2 (\varepsilon_{ij})^D (\varepsilon_{ij})^D < k^2 \ ,$$
$$\Phi(\varepsilon^D) = k((2(\varepsilon_{ij})^D (\varepsilon_{ij})^D)^{1/2} - k/2G) \quad \text{for}$$
$$2G^2 (\varepsilon_{ij})^D (\varepsilon_{ij})^D < k^2 \ ,$$

Ω is the domain with a boundary Γ, Γ_p is the part of Γ where the tractions are prescribed, f is the function of volume weight, p are tractions, $(\varepsilon_{ij})^D = (\sigma_{ij})^D / 2G$ are components of the strain deviatory tensor and κ is the bulk modulus. The minimum of the functional is sought for such displacements u, which fulfil the geometric boundary conditions.

In order to make more transferable the TFA and the improved concept using Desai idea, a uniaxial stress-strain distribution is depicted in Figure 1. One can observe that first the elastic problem is solved, where even not too precise values of material properties are required. From the second picture in Figure 1 it is seen that nonlinear material behaviour is estimated and the relaxation stresses improve the constitutive law in accordance with measurement.

2.1.3. TFA & DSC CONCEPT

Recall first the TFA involving the DSC. The transformation field analysis consists of expressing the stress σ at an arbitrary point ξ of the domain by virtue of superposition of stress $\sigma^{ext}(\xi)$ at ξ due to external loading which is applied to a plastic, visco-plastic, or other materials, and a linear hull of, say, the eigenstresses λ_1 and plastic strains ε^{pl} at other points x. Since we assume that at each point six values of stress, plastic stress, and eigenstress tensors are prescribed, the relation stresses σ^k at the points B_k, $k = 1,...,m$, and the eigenstresses and plastic stresses λ_1^l, $l = 1,...,n$ and $(\sigma^{pl})^l$, $l = 1,..., m$ at A_l becomes (to simplify the expressions the vector notation for stress and strain tensors is used), cf. (1):

$$(\sigma_i)^k = (\sigma_i^{ext})^k + \sum_{j=1}^{6}\sum_{l=1}^{m} (T_{ij}^{\sigma})^{kl} \ (\sigma_j^{rel})^l + \sum_{j=1}^{6}\sum_{l=1}^{m} (R_{ij}^{\sigma})^{kl} \ (\lambda_j)^l \ ,$$
$$i = 1,...,6, \ k = 1,...,m \quad (10)$$

or

$$(\sigma_i)^k = (S_i^{\sigma})^k + \sum_{j=1}^{6}\sum_{l=1}^{m} (R_{ij}^{\sigma})^{kl} \ (\lambda_j)^l \ ,$$
$$i = 1,.,6, \ k = 1,.,m \quad (11)$$

where $(S^{\sigma}_i)^k$ express the current state of the overall stresses involving nonlinear changes in the material.

Note that similar relations can be written for displacements:

$$(u_i)^k = (u_i^{ext})^k + \sum_{j=1}^{6}\sum_{l=1}^{m} (R_{ij}^{u})^{kl} \ (\lambda_j)^l + \sum_{j=1}^{6}\sum_{l=1}^{m} (T_{ij}^{u})^{kl} \ (\sigma_j^{rel})^l \ ,$$
$$i = 1,...,6, \ k = 1,...,m \quad (12)$$

or

$$(u_i)^k = (S_i^{u})^k + \sum_{j=1}^{6}\sum_{l=1}^{m} (R_{ij}^{u})^{kl} \ (\lambda_j)^l \ ,$$
$$i = 1,.,6, \ k = 1,...,m. \quad (13)$$

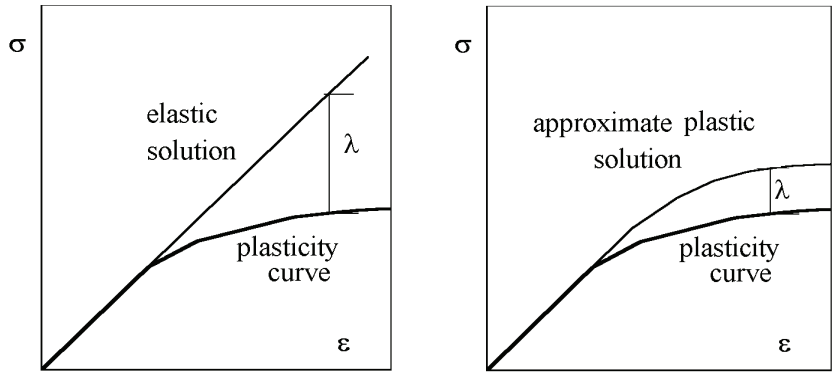

Fig. 1 TFA model and unified DSC & TFA model.

On the other hand measured stresses $(\sigma_i^{\text{meas}})^k$, or measured displacements $(u^{\text{meas}}{}_i)^k$ are available in a discrete set of points. A natural requirement is that the values of measured and computed values be as close as possible. This leads us to the optimization of an "error functional"

$$I[(\lambda_j)^l] = \sum_{i=1}^{6}\sum_{k=1}^{m}[(\sigma_i)^k - (\sigma_i^{meas})^k]^2 \to \min \qquad (14)$$

or

$$I[(\lambda_j)^l] = \sum_{i=1}^{6}\sum_{k=1}^{m}[(u_i)^k - (u_i^{meas})^k]^2 \to \min \qquad (15)$$

Differentiating I by $(\lambda_\alpha)^\beta$ yields a linear system of equations for $(\lambda_j)^l$:

$$\sum_{j=1}^{6}\sum_{l=1}^{m}(A_{\alpha j})^{\beta l}(\lambda_j)^l = Y_\alpha^\beta\,,\ \alpha = 1,..,6,\ \beta = 1,..,m, \qquad (16)$$

where

$$(A_{\alpha j})^{\beta l} = \sum_{i=1}^{6}\sum_{k=1}^{m}(R_{ij})^{kl}(R_{i\alpha})^{k\beta}\,,$$

$$Y_\alpha^\beta = -\sum_{i=1}^{6}\sum_{k=1}^{m}[(S_i)^k - (u_i^{ext})^k] +$$

$$+\sum_{j=1}^{6}\sum_{l=1}^{m}(R_{ij})^{kl}(\lambda_j)^l(R_{i\alpha})^{k\beta}$$

In order to get $\mathrm{d}(\sigma_i)^k$ in (3), one needs to calculate $\mathrm{d}(\lambda_j)^l$. This is the difference between $(\lambda_j)^l$ from (16) and the same quantities from the previous step of incremental method.

The procedure deserves a closer attention. In the first step the influence matrices are created, as described in the above explanation (Sect. on formulation of the TFA). The distribution of the disturb function D is determined mostly from laboratory tests. The incremental method is recommended when applying the DSC & TFA.

Let us start with some load of the trial body.

At the beginning the FA state will be most probably not reached. The Intact State follows the von Mises-Huber-Hencky law. When increasing the load, the DSC has to involve both IS and FA states into the computation. Then, the stresses are split into IS and FA parts. Increments of both these parts can be done from the DSC and the total stress for both parts is given by adding the increments to the previous steps. The same is valid for the total current stress; see (11).

Since the relations (16) are linear, substitutions of $(S_i)^k$ and $(\lambda_i)^k$ does not change the linearity. Then applying the minimum condition for the additional eigenstresses, the improvement of current stresses or error for the DSC is obtained.

The above-described procedure can be created for measured displacements in a similar way. The displacements have to substitute overall stresses and the "error functional" has to be employed. This is not in the full compliance with classical Transformation field analysis, but it follows from mechanical point of view.

2.1.4. CLASSICAL DAMAGE CONTINUUM MODEL

In the previous section, λ_1 was used to express "error function", improving the choice of plasticity model. The function λ_2 will express the influence of the damage.

In the continuum damage model it is assumed that the damaged parts can carry no stress at all, and they act as voids. In other words, the observed response derives essentially from the undamaged parts; their stress-strain-strength behaviour is degraded because of the existence of the damaged parts. For example, the damage parameter, ω, is defined as

$$\omega = 1 - \frac{V^V}{V} \qquad (17)$$

where V^V is the volume of the damaged parts and V is the total volume of the material element. Then, $\omega = D$ represents the special case and appears in λ_2 as an argument.

In the sense of the Unified TFA & DSC model the equilibrium for $\mathrm{d}\sigma$ can be written as

$$\sigma = \sigma^{IS} - \lambda_2(\omega)\,,$$

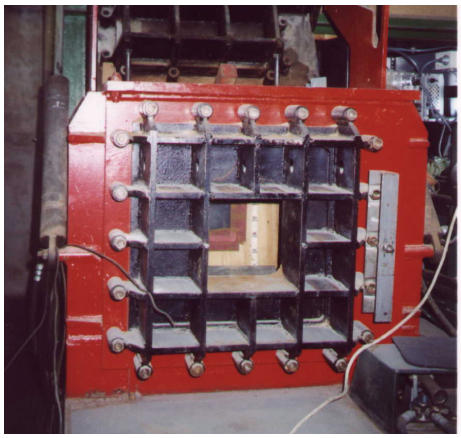

Fig. 2 View at a face of the stand.

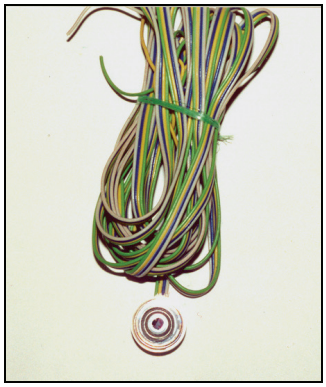

Fig. 3 Semiconductor transducer.

The representation of the function of $\lambda_2(\omega)$ can be found in (Kachanov, 1992), for example.

2.2. EXPERIMENTAL MODEL TESTS

Series of the scale physical models were constructed on a scale of 1 : 20 in modelling stand with dimensions 500 x 500 x 570 mm (Fig. 2). Modelled tunnel of cylindrical shape had inner diameter 80 mm. The longitudinal axis of the tunnel was put 200 respectively 300 mm under the model surface symmetrically with respect to the sidewalls of the stand.

In used scale, modelled tunnel represented utility tunnel with diameter of 1.6 m in the depths of 4 m (respectively 6 m) under the surface (Trčková, 2005). The tunnels were stiffened by an equivalent of a real lining with various strengths prepared from hardened paper with the thicknesses of 0.2, 1.6, and 3.4 mm. An equivalent material used for constructing models, was created by compound of siliceous sand, bentonite and fat. The applied equivalent material is very plastic with a high rate of permanent deformation and on the model scale produced consolidated soils of the mudstone type.

Monitoring of the stress changes around the tunnel was carried out by semiconductor transducers, which measure the stress applied perpendicular on their bearing surface (Fig. 3).

The external loading representing strip footing was applied on the model surface in width equality to diameter of the tunnel parallel, respectively perpendicular with longitudinal axes of the tunnel and in all length, respectively width, of the model stand.

2.2.1. STRESS DISTRIBUTION IN DEPENDENCE ON INCREASING EXTERNAL LOADING OF THE TUNNEL

A model of the tunnel lined by lining of 1.6 mm thickness was constructed and the redistribution of horizontal and vertical stresses in the neighbourhood of the tunnel due to external loading representing strip footing was studied. The external loading by metal

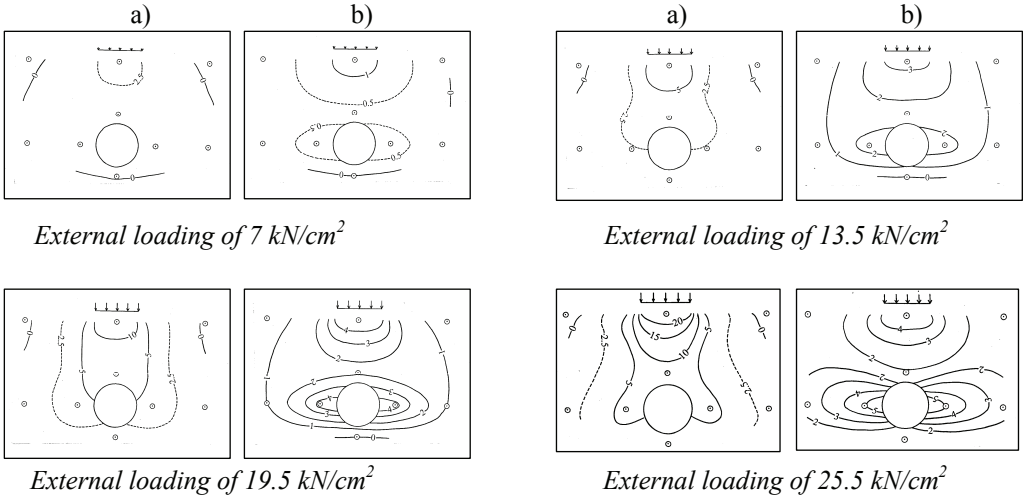

Fig. 4 Stress distribution (in kPa) due to successively increasing external loading; (a) vertical stress, (b) horizontal stress**.**

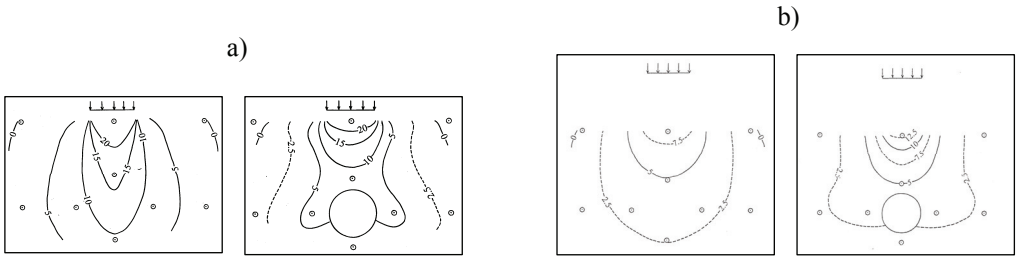

Fig. 5 Vertical components of the stress redistribution (in kPa) in dependence on two tunnel depths under surface; (longitudinal tunnel axis of 200 mm (a) and 300 mm (b) under the model surface). Strip footing is parallel to the longitudinal axes of the tunnel. Tunnel lining thickness was of 1.6 mm.

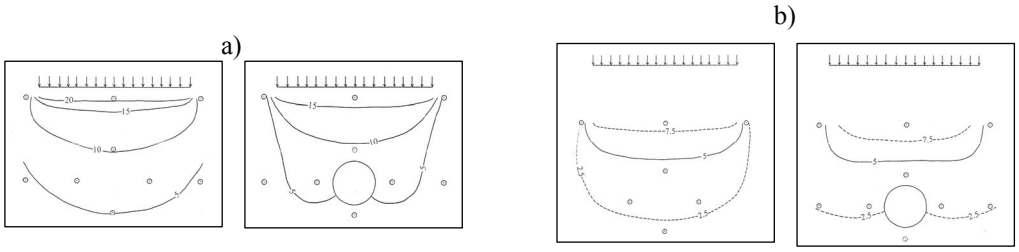

Fig. 6 Vertical components of the stress redistribution (in kPa) in dependence on two tunnel depths under surface; (longitudinal tunnel axis of 200 mm (a) and 300 mm (b) under the model surface). Strip footing perpendicular to the longitudinal axes of the tunnel. Tunnel lining thickness was of 1.6 mm.

weights was applied in this case parallel with longitudinal axes of the tunnel and successively increased. The results of this experiment demonstrate expansion of domains affected by equivalent of the strip footing of various weights.

2.2.2. STRESS DISTRIBUTION IN DEPENDENCE ON THE TUNNEL DEPTH UNDER THE SURFACE

To find stress redistribution in the neighbourhood of the tunnel due to various tunnel depths under the surface, further models were constructed. The models about 100 mm higher, one without a tunnel and second with the tunnel with longitudinal axis of 300 mm under the model surface were prepared. The semiconductor transducers stayed on the same place as in the previous models, i.e. in the same places with respect to tunnel position.

The tunnel lining was prepared from hardened paper with thickness of 1.6 mm. In this case, models were loaded once again parallel with longitudinal axis of the tunnel and loading successively increased up to 25.5 kN/cm^2. In comparison with results obtained in the previous model, it proved to be equivalent material of overburden absorbed part of the stress caused by strip footing loading.

2.2.3. STRESS DISTRIBUTION IN DEPENDENCE OF STRIP FOOTING LOCATION WITH RESPECT TO THE LONGITUDINAL AXIS OF THE TUNNEL

Series of similar scale models were prepared to assess an influence of strip footing location with respect to the tunnel longitudinal axis to redistribution stresses around the tunnel. The increasing external loading of the models, representing strip footing, was realized perpendicular with longitudinal axis of the tunnel.

The models were constructed like with tunnel axis placed 200 mm as 300 mm under the model surface. Tunnel lining was chosen equal of 1.6 mm thickness for these models. Also two models without tunnel were prepared, first one lower and second one about 100 mm higher. In comparison with the Figures 5 and 6 it is possible to see changes between stress distributions in dependence on the strip footing location with respect to the longitudinal axis of the tunnel.

2.3. RESULTS

It has been shown that the strength of the equivalent of the concrete lining, depth of the tunnel under surface and location of the strip footing principally influence distribution of the stress. Some

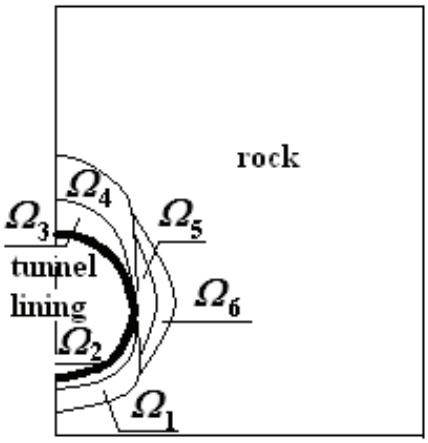

Fig. 7 Distribution of eigenstrain zones.

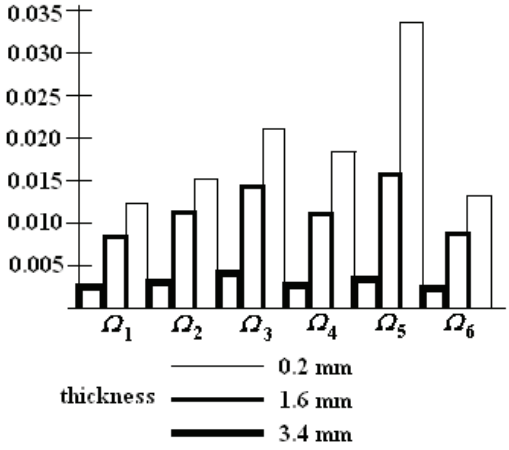

Fig. 8 Spectral values of eigenstrain tensors in the zones; various thicknesses.

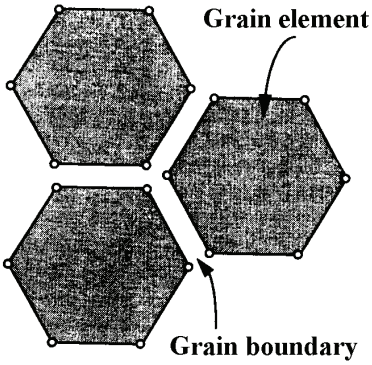

Fig. 9 Sample decomposition - three adjacent particles in mutual contact.

range of relative stiffness was considered in our study for a typical location of small tunnels.

The reason, wherefore first of all described scale physical models were carried out, was to use results from physical scale models in numerical modelling.

In the same way as experiments, numerical examples were prepared. Six zones, Ω_1, Ω_2,…, Ω_6, were selected according to Figure 7. The Unified model started from the thickness 3.4 mm, and plastic behaviour together with damage were created. The tunnel linings changed in the sense of experimental models.

Additional eigenstrains are depicted in Figure 7. It is seen that if the thickness is weaker, the effect of opening (concentration of plastic strains) appears in zone Ω_5, while in other zones eigenstrain slightly increases (Fig. 8). They can be lowered after more precise selection of the Unified model.

3. SOLUTION OF STRUCTURAL STRENGTH BY FREE HEXAGON METHOD

The free hexagon method seems to be one of very promising (Cundall, 1971; Moreau, 1994). In comparison with previous methods, this method involves time-dependent problem with Newtonian forces, which are caused by contact forces of moving particles. It simplifies the body of the earth (soil) to a set of hexagons, which are, or are not in a mutual contact. The material properties of the hexagons are determined from the state of stresses. Adjusting the idea of PFC (particle flow code), which starts with balls instead of hexagons and dynamical equilibrium, while in our case the static equilibrium is considered. The hexagons represent a typical shape of grains the earth consists of. The method was used to assess structural strength below foundation.

The behaviour inside each element is either linear or non-linear (plastic, viscoelastic, viscoplastic, etc). To describe such behaviour, boundary elements are applied. The static equilibrium is used in formulation of free hexagon method. This method has been established in middle 90-ties and the fundaments can be found in Procházka and Válek, 2000.

The experimental models are based on physically equivalent materials and scale modelling. Physical model on a scale of 1 : 25 was prepared. In our case similar modelling was used with such an exception that very particular materials were used.

3.1. NUMERICAL MODELLING

3.1.1. COMPUTATIONAL MODEL IN STATIC STATE

The free hexagon element (particle) method is briefly described for static state. For more details see e.g. (Procházka, 2003). A cut from arrangement of hexagonal elements that are in mutual contacts is seen from Figure 9.

When dealing with a crack in general, two principal methods are used. First, the means of fracture mechanics are applied, or contact problem can be formulated. The first case is generally not suitable to us, because the direction or way of propagation of the cracks should not be known in advance.

In this paper the second possibility is utilized and the obstacle of unknown propagation of the cracks is avoided by creating free hexagonal particles, which are in mutual contact in undeformed state, but can be disconnected because of violating contact conditions.

Let the distribution of both displacements and tractions along the boundary of the trial element are linear (this approximation is admissible when using the BEM), while the FEM does not admit such an approximation: tractions are polynomials of degree lower by one when comparing them with displacements. Moreover, it is well known that such a distribution fulfills the convergence condition (if the diameter of the element tends to zero, the approximation tends to "continuous" solution). Generally, the problem of elasticity can be written in Ω (the domain of one particle with boundary Γ) as:

$$\sum_{l=1}^{2} c_{kl}(x)u_l(\xi) = \sum_{i=1}^{2}\sum_{s=1}^{6}\int_{\Gamma_s} p_i(x)u_{ik}^*(x;\xi)d\Gamma(x) -$$
$$-\sum_{i=1}^{2}\sum_{s=1}^{6}\int_{\Gamma_s} u_i(x)p_{ik}^*(x;\xi)d\Gamma(x) +$$
$$+\sum_{i=1}^{2}\int_{\Omega} b_i(x)u_{ik}^*(x;\xi)d\Gamma(x)$$
$$\xi \in \Gamma,\ k = 1, 2, \qquad (18)$$

where Γ_s is the boundary of one side of the element, c_{kl} is a square matrix depending on a position of $\xi \in \Gamma$, u_i and p_i are displacements and tractions, respectively, which are projected to the coordinate directions, and the quantities with asterisk are given kernels. If the point ξ is positioned successively at the centers of six boundary elements (along which the distribution of displacements and tractions is uniform), twelve equations are obtained relating 6^2 displacements and 6^2 tractions and 6 components of the volume weight.

Eqs (18), written for the relations on the boundary, are then simplified as:

$$\frac{2}{3}\sum_{l=1}^{2}\delta_{kl}u_i(\xi_t) = \sum_{i=1}^{2}\sum_{s=1}^{6} p_i\int_{\Gamma_s} u_{ik}^*(x;\xi_t)d\Gamma(x) +$$
$$+\sum_{i=1}^{2}\sum_{s=1}^{6} u_i\int_{\Gamma_s} p_{ik}^*(x;\xi_t)d\Gamma(x) + \sum_{i=1}^{2} b_i\int_{\Omega} u_{ik}^*(x;\xi_t)d\Gamma(x)$$
$$\xi \in \Gamma,\ k = 1, 2,\ t = 1,\ldots,6, \qquad (19)$$

where ξ_t are vertices of the boundary elements. The kernels denoted by asterisks are given.

Now define vectors $\alpha^j, \beta^j, j = 1,...,6$, which are created as:

$$\alpha^j = \begin{pmatrix} u_x^j \\ u_y^j \end{pmatrix}, \quad \beta^j = \begin{pmatrix} p_x^j \\ p_y^j \end{pmatrix}. \qquad (20)$$

Using this notation the relation on the elements can be recorded as:

$$A\alpha = B\beta + \bar{b} \qquad (21)$$

where the matrices are created from discretization of the particle boundary of the first and second integral RHS in (19). Eventually the vector $\bar{b}$ is a consequence of discretization of volume weight forces to the boundary elements. The matrix A is generally singular, while the matrix B is regular. This fact enables one to rearrange equation (21) into the form:

$$K\alpha = \beta + b, \quad K = AB^{-1} \qquad (22)$$

The relation displacements - tractions is obtained by (22). In this way, the discretized problem turns to the problem similar to the FEM.

Let us concentrate on boundaries of two adjacent elements. In a plane, a simple transformation rule is valid:

$$\begin{pmatrix} p_n^j \\ p_t^j \end{pmatrix} = \begin{bmatrix} \cos\phi_i & \sin\phi_i \\ -\cos\phi_i & \cos\phi_i \end{bmatrix}\begin{pmatrix} p_x^j \\ p_y^j \end{pmatrix} = T\begin{pmatrix} p_x^j \\ p_y^j \end{pmatrix}, \qquad (23)$$

Moreover, we denote by p_n^{ij} the tractions in the normal direction for the element i being in contact with the element j. Similarly, p_t^{ij} are the tangential traction on the interface of elements I and j, $\Delta_n^{ij} = u_n^{ij} - u_n^{ji}$, $\Delta_t^{ij} = u_t^{ij} - u_t^{ji}$ are differences of displacements in normal and tangential directions, respectively, in local coordinates, which are created in such a way that the normal is the outward unit normal to the element with lower number in global numbering and the tangent creates with the normal right-rotational system. If we decide that the number of the side k lies between nodes k and $k + 1$, $k = 1,,,5$, and the side number 6 is positioned between nodes 6 and 1, the relation in numbering of sides and nodes is unique. Under these assumptions the equation (23) can be rewritten as:

$$\begin{pmatrix} p_n^{ij} \\ p_t^{ij} \end{pmatrix} = \begin{bmatrix} \cos\phi_{ij} & \sin\phi_{ij} \\ -\cos\phi_{ij} & \cos\phi_{ij} \end{bmatrix}\begin{pmatrix} p_x^{ij} \\ p_y^{ij} \end{pmatrix} = T\begin{pmatrix} p_x^{ij} \\ p_y^{ij} \end{pmatrix}, \qquad (24)$$

where φ_{ij} are oriented angles from x-direction of the local normal (by definition this normal in taken with respect to the edge of an element with the lesser number). Since we decide that in the undeformed state the nodes (edges) are connected by springs with very high stiffness s, one can write the linear spring rule in the form:

$$\begin{pmatrix} p_n^{ij} \\ p_t^{ij} \end{pmatrix} = \begin{bmatrix} s_n^{ij} & 0 \\ 0 & s_t^{ij} \end{bmatrix}\begin{pmatrix} \Delta_n^{ij} \\ \Delta_t^{ij} \end{pmatrix} = T\begin{pmatrix} p_x^{ij} \\ p_y^{ij} \end{pmatrix}, \qquad (25)$$

In what follows we introduce the denotation of the adjoin elements in contact by their numbers written in superscripts. Along arbitrary adjoin abscissas we then write:

$$\beta^{ij} = \begin{pmatrix} p_x^{ij} \\ p_y^{ij} \end{pmatrix} = \begin{bmatrix} s_{xx}^{ij} & s_{xy}^{ij} \\ s_{yx}^{ij} & s_{yy}^{ij} \end{bmatrix} \begin{pmatrix} \Delta_x^{ij} \\ \Delta_y^{ij} \end{pmatrix} = s_{ij}(\alpha^{ij} - \alpha^{ji}) \tag{26}$$

where notation from (20) has been adopted and

$$s_{xx}^{ij} = s_n^{ij} \cos^2 \varphi_{ij} + s_t^{ij} \sin^2 \varphi_{ij}$$
$$s_{yy}^{ij} = s_t^{ij} \cos^2 \varphi_{ij} + s_t^{ij} \sin^2 \varphi_{ij}$$
$$s_{xy}^{ij} = 1/2\left(s_n^{ij} - s_t^{ij}\right) \sin 2\varphi_{ij}$$

and Δ_x^{ij} and Δ_y^{ij} are differences of displacements in respectively x and y directions in the elements i and j, i.e., $\Delta_x^{ij} = u_x^{ij} - u_x^{ji}$, $\Delta_y^{ij} = u_y^{ij} - u_y^{ji}$

Note that

$cos^2 \phi_{ij} = cos^2 \phi_{ji}$, $sin^2 \phi_{ij} = sin^2 \phi_{ji}$, $sin 2\phi_{ij} = sin 2\phi_{ji}$.

Holding the assumption of the hexagonal shape of all elements (not necessarily of the same area), if the element k and l are in contact, then the i-th edge of k is in contact with i+3-rd mod 6 edge of the element l . It means that 1-4, 2-5, 3-6, 4-1, 5-2, and 6-3 are exactly numbers of sides in contact. Using the equilibrium along the edges and action-reaction law we eventually get:

$$\beta_i^s\left(element\ \ k\right) + \beta_i^s\left(element\ \ l\right) = s_i^{kl}\left(\alpha_i^{kl} - \alpha_i^{lk}\right) = \\ = \left(k_{ij}^{kl} - \delta_{ij} s_i^{kl}\right)\alpha_j^{kl} + \left(k_{ij}^{lk} - \delta_{ij} s_i^{lk}\right)\alpha_j^{lk} \tag{27}$$

Kronecker´s delta δ^{ij} has been used. The system of the type (27) is created for each edge, for proper angle φ to determine. It means that two equations of the type (27) for the boundary nodal point i and i+1 (when apply the boundary edge i in our notation) are valid.

3.1.2. INTERFACE CONDITIONS

Considering the most of particles are of the same, or of similar shape, very powerful iterative procedure can be applied, and the stiffness matrix (following from boundary integral formulation on the hexagonal particles) can be stored into the internal memory of computers. The hexagonal particles may be studied under various contact (interfacial) conditions of the grain particles (elements). In out paper generalized Mohr-Coulomb hypothesis with exclusion of non-admissible tensile stresses along the contacts is used.

The problem formulated in terms of hexagonal elements enables one to simulate the way of propagation of cracks and the extrusion of rock elements. The cracking of the medium can be described in such a way that the local damage may be derived. Also local deterioration of the material can be seen from the pictures, drawn for particular examples. Such a movement of displacements and flow of stresses cannot be probably obtained from continuous numerical methods.

Starting moment of debonding is simulated as follows: we first consider the bonded state with very high penalty (spring stiffness); if along one boundary abscissa the contact rules are violated, no penetration of adjacent elements is admissible, but mutual movement of the abscissas is allowed.

3.2. EXPERIMENTAL MODEL

Experimental part was focused on construction of physical model on a scale 1 : 25, in a model stand with dimensions 870 x 265 x 595 mm. On the assumptions that drop-out is symmetrical; only one half of the drop-out was modelled so that front wall of the model stand cut in two modelled drop-out (Fig. 10).

Drop-out foot on the model was 120 x 60 mm, with depth of 120 mm. The model was loaded up to 20 kN/cm^2 by metal weights, respectively by leaden balls on the foot of the drop-out in surface with dimensions 80 x 40 mm.

During model construction 18 semiconductor transducers were placed around the drop-out in the vertical planes passing through the drop-out into the model to measure stress changes due to loading. Leadingin cables were conducted to the back wall of the model (Fig. 11).

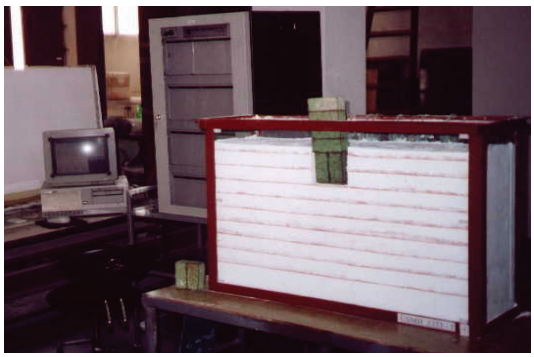

Fig. 10 View of the model stand during experiment.

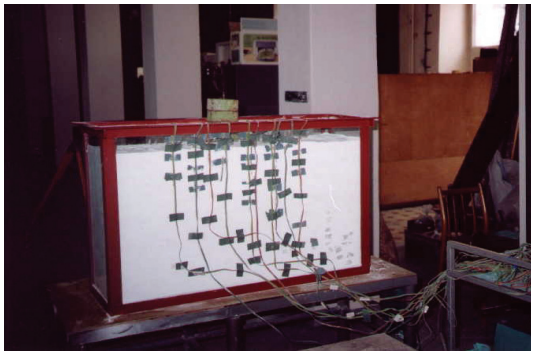

Fig. 11 Back wall of the model with cabling of semiconductor transducers.

Table 1 Comparison of measured and computed values of vertical stresses.

	Vertical stress changes (kPa)								
	1	2	3	4	5	6	7	8	9
Measured	-8	-7.5	-6	-2	0	1.5	-7	-6.5	-2
Computed	-7.35	-7.25	-5.92	-2.34	0.15	1.78	-7.26	-6.28	-1.89
	Vertical stress changes (kPa)								
	10	11	12	13	14	15	16	17	18
Measured	-0.5	0	1.5	-4	-3	-2	0	0.5	0
Computed	-0.68	0.23	1.48	-4.2	-3.42	-2.21	0.14	0.12	0.22

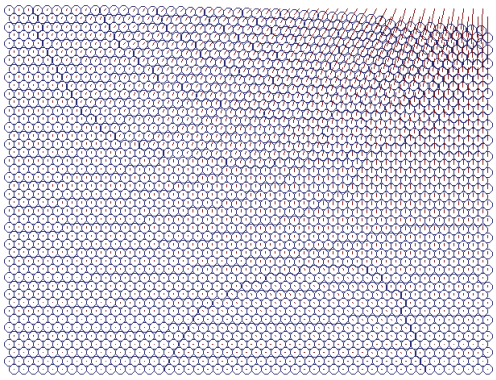

Fig. 12 Displacements due to loading on the terrain.

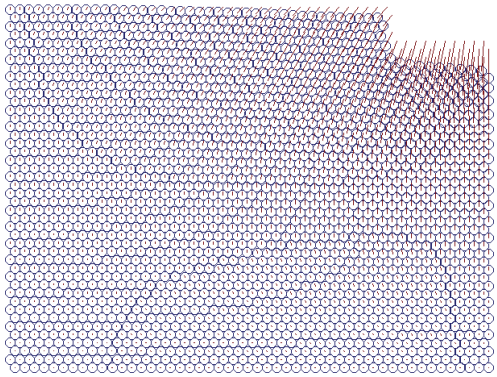

Fig. 13 Displacements due to loading 50 cm below terrain.

3.3. EXAMPLE AND RESULTS

An example is discussed to show the possibilities of the method put forward in this text. The geometry of at most 2200 hexagonal elements is seen in Figure 12. Since the load on the upper part of 6 m wide is induced, and is relatively very high (8 MPa), the volume weight may be neglected and only one half (the left one) of the subsoil may be considered. Long strip (ditch) is considered, so that two dimensional cases are considered.

Material coefficients are: E = 1 GPa, G = 0.1 GPa, shear strength c = 1 MPa and tensile strength p_n^+ = 10 kPa.

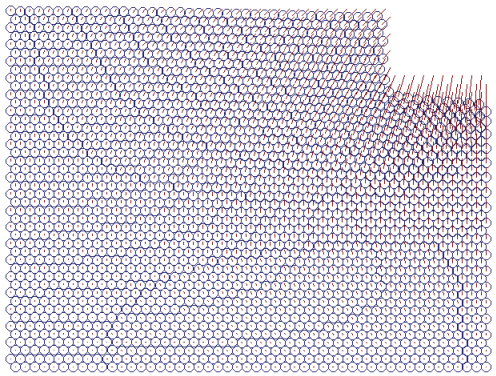

Fig. 14 Displacements due to loading 100 cm below terrain.

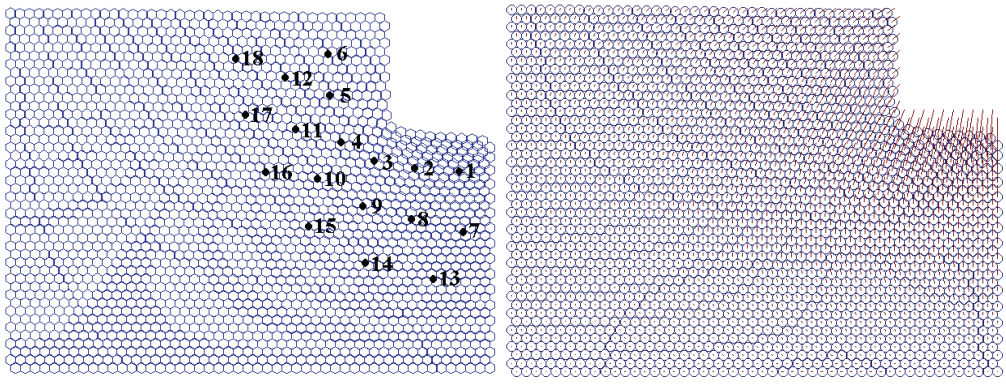

Fig. 15 Displacements due to loading 150 cm below terrain, measurement and computation - see Table 1.

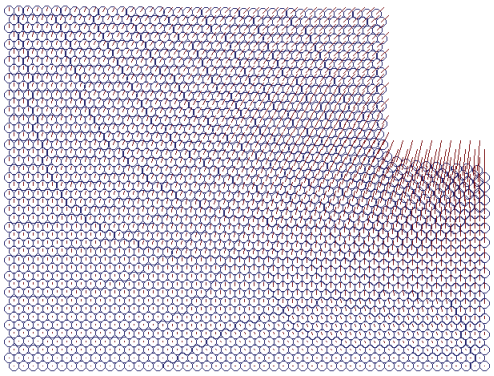

Fig. 16 Displacements due to loading 200 cm below terrain.

In Figure 13 the movements are shown. The influence of loading is negligible about 6 m below the loading strip. Figs. 14 and 15 show the movements for a ditch of 500 mm and 1000 mm respectively. It is observed that no change in structural strength appears. To the pattern with the ditch 1500 mm a model from physically equivalent materials was prepared and the results from both methods were compared.

The results in MPa are introduced in Table 1. The appropriate pictures, Fig. 15 and Fig. 16 prove a principal drop of structural strength. This is an impact of approaching stiff rock bed. The side of the ditch is in tension in some locations, as the loading causes swelling the soil. This is valid for ditches from 0.5 m lower.

The proposed model, in contrary to modern numerical methods (FEM, BEM, etc.), is enable one to disconnect the medium described by the balls, when needed (e.g. providing certain requirement on tensile strength). The most natural contact conditions - Mohr-Coulomb hypotheses - may be simply introduced and, after imposing all such contact conditions.

4. BACK ANALYSIS OF REINFORCED SOIL SLOPES

Among the most popular reinforcement in soil mechanics of slopes is anchoring and nailing. In our experiments nails are applied; they are penetrated into the slope, it is loaded only by its volume weight. The material of nails as well as that of the slopes is known from laboratory tests. This circumstance influences the distribution of stresses along the length of the body of the nail. Moreover, position of the nails to the stability of the reinforced slopes is observed. As the experiments are carried out in scale models, similarity conditions have to be obeyed. The technology of construction of experimental models is very important. Similarity rules are applied, but in this case no additional tests on physically equivalence of materials (real and that in the scale model) are necessary. As is well known, slopes stability is phenomenon which underlies the softening material behaviour, i.e. the nonlinear behaviour is concentrated along the slip curve. All kinds of nails are fully active after their mobilization. Different position of nails is considered to obtain the influence of this effect.

In numerical analysis a priori integration method is fully used (Koudelka and Procházka, 2001). Its application enables one to decide relatively very quickly if the slope is stable or the measure of stability, the safety margin.

4.1. BASIC PRINCIPLES OF A PRIORI INTEGRATION METHOD (AIM)

The idea of the AIM arose from the needs of design practice. In the design of big excavations or embankments which occurred, e.g., in the construction of the underground railway it was found suitable to base the actual design on parametric studies depending on the simplified geometry of the slope and the geotechnical parameters of the soil of which the slope consists. Computations have shows explicitly that for reasons of final assessments of slope stability it was impossible to use modern numerical methods (finite element method, boundary element method). However, classical slice methods did not appear entirely suitable, either. Modern methods need more computational time, while slice methods are numerically unstable and do not enable the application of minimization strategy for a more accurate stability coefficient computation.

One of the possibilities of elimination of these shortcomings consists in the application of the AIM, e.g., to the classical plain gravity model which has the advantage of explicit expression of the stability coefficient on the given shear surface, can easily be extended to three dimensions and involve other influences on the slopes.

Before presenting the initial formulas we introduce some symbols and assumption. First we will deal with two-dimensional problems in *Oxy* coordinate system. In practice it is advantageous to locate the origin of the coordinates *O* at the toe of the slope. The application of the AIM consists in expressing the problem in functional form. For the classical model, for instance, we seek the stability measure (safety factor) on a concrete admissible shear surface with the understanding that the safety factor is the minimum of stability measures. Moreover, in the AIM we express the functionals for a fixed shear surface in the form of functions. This can be achieved, e.g., with the assumption (frequently used in engineering practice) that geotechnical parameters are homogeneous and isotropic by parts (by layers). In our case homogeneous medium is considered, as the influence of nails is studied in the scale model.

Let $y = t(x)$ be the boundary of the slope surface (terrain) and $y = f(x)$ describe the shear surface the admissible form of which is a part of the circle. In order not to complicate the explanation, let us assume that f is a function, i.e. that there is just one value of

y for every x within the admissible interval. The generalization of this assumption is not connected with any difficulties. Further, in accordance with the principal idea of the model (equilibrium on the fixed shear surface together with the respective denotations is shown in Figure 17) it is possible to define the safety factor F on the shear surface as follows:

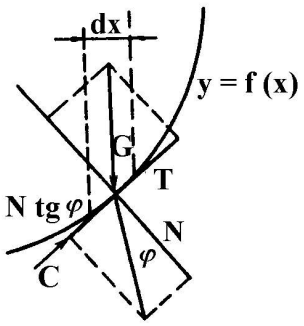

Fig. 17 Equilibrium of forces on the shear surface in the gravity model.

$$F = \frac{N\tan\phi + C}{T} \tag{28}$$

where N and T are the normal and tangential components, respectively (with reference to the shear surface) of the unit weight of the soil above the shear surface, ϕ is the angle of internal friction (shearing resistance) and C is the cohesion.

The most probable location of the shear surface and simultaneously the safety factor value (minimum safety factor) are determined by the minimization of the values of F, i.e.

$$F_0 = \text{ minimum } F \tag{29}$$

where the minimum is considered across all admissible shear surfaces, i.e. such circles for which the set of those x for which

$$S(x) = P_+[t(x) - f(x)] \neq 0 \tag{30}$$

is not empty. In the definition of the function S we have introduced the Heaviside operator

$$P_+[a] = 1 \quad \text{for} \quad a > 0\,, \qquad P_+[a] = 0 \qquad \text{otherwise} \tag{31}$$

The condition (30) means that the diagrams of the functions t and f and intersect at least in two points and $t(x_0) > f(x_0)$ at least for one x_0. The condition (29) determines the form (or, to be exact, the location) of the shear surface along which the slip will occur most probably, if the safety factor F_0 is lower than the respective safety factor of the slope, determined either by a standard (EC7-1, DIN, CSN), or by the designer's experience. If the safety factor is higher than this number, the slope can be considered stable.

Now we can express the individual terms in (28) as follows:

$$T(f) = \int_{-\infty}^{\infty}\int_{f(x)}^{t(x)} \gamma(x,y)\,p(x)\,S(x)\,dy\,dx,$$

$$C(f) = \int_{-\infty}^{\infty} \frac{c(x)}{q(x)} S(x)\,dx$$

$$N\tan\phi(f) = \int_{-\infty}^{\infty}\int_{f(x)}^{t(x)} \gamma(x,y)\tan\phi(x)\,q(x)\,S(x)\,dy\,dx \tag{32}$$

where γ is the volume weight of the soil, c is the cohesion, and

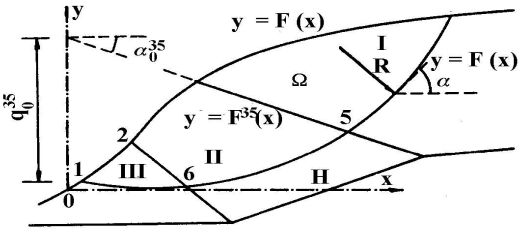

Fig. 18 Topological relations of the AIM.

$$p(x) = \frac{x - x_C}{R}, \quad q(x) = \sqrt{1 - p^2} \tag{33}$$

where (x_C, y_C) are the coordinates of the center of the slip surface and R is its radius. Note that the functions p and q in (6) are the sine and cosine, respectively of the angle α between the tangent to the slip surface at the point $(x, \sqrt{R - (R^2 - (x - x_C)^2})$ and the axis x (see Fig. 18). The material constants φ and c can be entered as residual or peak values. In this way it is possible to consider also the influence of deformation. Description of the geometry and subregions, the procedure of the AIM can be applied, is seen from Figure 18. Roman numerals denote homogeneous and isotropic subdomains (elements), Arabic numerals describe the vertices of element boundaries. It can easily be verified that the formulas (32) correspond with the relations of the gravity model for the case of limit transition in the meaning of the Riemann integral definition.

The cases most frequently occurring in practical computations are the cases of soil mass, the boundary of which can be approximated by a polygon and the material of the mass is homogeneous and isotropic in parts, while these parts (subdomains) are also bounded by polygons.

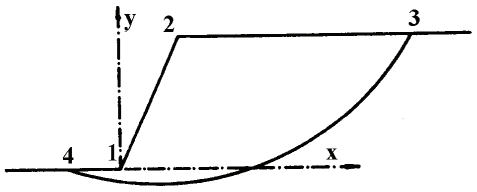

Fig. 19 Geometry of the simple slope.

In order to study the influence of reinforcing nails, simple slope, i.e. a homogeneous isotropic slope without benches, see Figure 19, is considered, and the slip curve meets the toe of the slope, i.e. points 1 and 4 are identical. This is the case of slopes with steeper toe angles. Our aim is the computation of the values of integrals (32) for the latter case. As in this particular case γ, φ and c are constant, so that it holds that

$$T = \gamma \left\{ \int_{x_1}^{x_2} t^{12}(x) p(x)\, dx + \int_{x_2}^{x_3} t^{23}(x) p(x)\, dx - \int_{x_3}^{x_1} f(x) p(x)\, dx \right\}$$

$$C = c \int_{x_1}^{x_3} \frac{dx}{q(x)}$$

$$N \tan\phi = \gamma \tan\phi \left\{ \begin{array}{l} \int_{x_1}^{x_2} t^{12}(x) q(x)\, dx + \int_{x_2}^{x_3} t^{23}(x) q(x)\, dx - \\ - \int_{x_3}^{x_1} f(x) q(x)\, dx \end{array} \right\} \quad (34)$$

where superscripts *ij* stands for abscissa or circle of the slip line $i - j$, i, j =1,2,3. Furthermore, in the last equations x_i and y_i are coordinates of point *i*. Substituting for the slope 1 - 2 and ridge 2 - 3 yields

$$t^{12}(x) = k_0 \ , \quad t^{23}(x) = q_0 \ , \quad f(x) = y_C - Rq(x) \quad (35)$$

where k_0 is the value of the slope and q_0 is the height of the ridge. We ascertain that the explicit expressions of *T, N* tan φ and *C* is split into an algebraic sum of influences of individual abscissas forming the boundary of the slope and its individual layers and the parts of the circles forming the slip surface.
Before coming to the explicit expression of influences from the integration over an abscissa or a circle it is advisable to introduce substitution (parameter *p* stands for sine of the angle α) and formulate functions:

$$x = x_C + pR \quad dx = R\, dp \quad F_1(p) = \frac{\left(\sqrt{1-p^2}\right)^3}{3}$$

$$F_2(p) = \frac{p^2}{2} \quad F_3(p) = \frac{\arcsin p + p\sqrt{1-p^2}}{2} \quad (36)$$

$$F_4(p) = \frac{p^3}{3} \quad F_5(p) = p - \frac{p^3}{3} \quad F_6(p) = \arcsin p$$

Now it easily follows that the influences from integrations below the abscissas can be expressed as (denoted by brackets):

$$\begin{array}{l} [T] = [AF_4(p) + BF_2(p)]_i^j \\ [N \tan\varphi] = [BF_3(p) - AF_1(p)]_i^j \tan\varphi \end{array} \quad (37)$$

where

$A = \gamma R^2, \quad B = \gamma R(k_0 x_C + q_0)$, and

$[f(p)]_i^j = f(p_j) - f(p_i)$, $p_i = (x_i - x_C)/R$.

In case of circular segments are considered the following formulas can be derived:

$$[T] = [AF_2(p) + BF_1(p)]_i^j$$

$$[N \tan\phi] = [AF_3(p) - BF_5(p)]_i^j \tan\phi$$

$$C = cR[F_6(p)]_i^j$$

where $A = \gamma R y_C, \quad B = \gamma R^2$. The loading from above the ridge is taken into volume weight, while the influence of the nail (nails) is an additional shear force at the cross of current slip circle and the nail. The value of it follows from the experiments. If instead of nail a geotextilie is put into the material of the slope, one force is needed to explain the influence of the reinforcement on the stability of the slope. This is not the case, so that different number of nails is necessary to consider. The aim of the coupled modelling consists in tuning the numerical model, turned to a programming code, in such a way that the influence of the nails can be identified with high accuracy.

4.2. PHYSICAL MODELLING AND RESULTS

Slope 1:1.5 (length : height) was considered in the scale of 1:100. The slope obeys the laws of geometrical and physical similarity which is inferred for a consideration of dimensional analysis, (Kožešník, 1983; Procházka and Trčková, 2000). Physically equivalent material was selected to be in compliance with selected real slope as: Mixture of ballotine and fat is the basic material for this laboratory tests, the contents of ballotine was 99.87%,

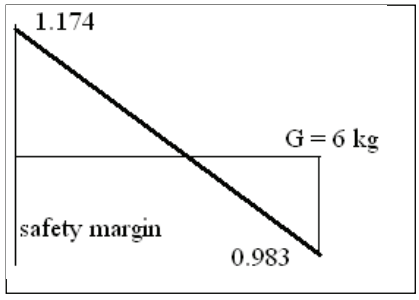

Fig. 20 Relation load and safety margin.

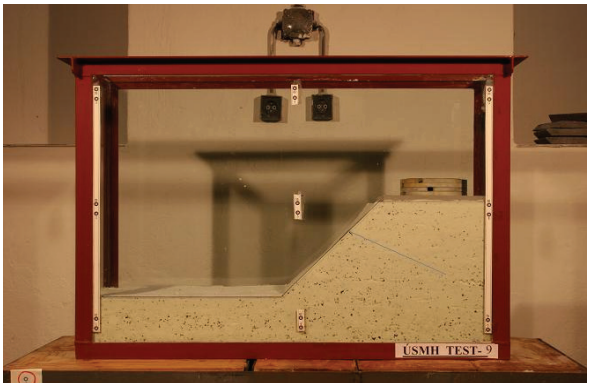

Fig. 21 View of stand with the slope loaded from above and with the first position of a nail.

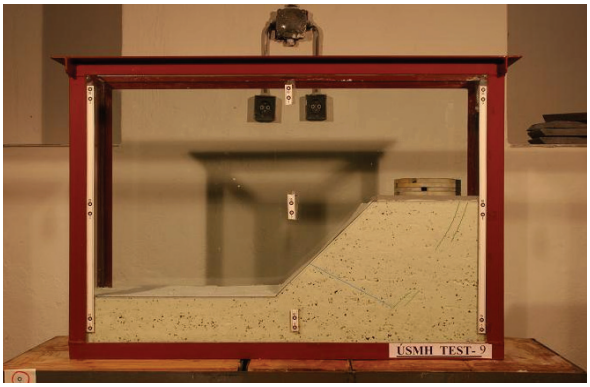

Fig. 22 The second type of reinforcement, slip curves highlighted.

fat A00 was 0.125%. The model was constructed in the stand with dimensions of 0.9 m x 0.29 m x 0.63 m.

The loading from above the ridge was applied to tune the material properties of the aggregate in the model (the slope created from the physically equivalent material together with a nail). The nails have been prepared from a chip of bamboo, unified in the shape and dimensions, their shear strength is known, so that the resistance force due to a nail is also given. Influence of load to the safety margin is depicted in Figure 20.

Two basic positions is horizontal set of nails were prepared. The first is seen in Figure 21, it should help to stiffen the upper part of possible slip surface (curve). As is well known, this is the most advantages position, since the slopes in general start their damage along the ridge. The first loading step is also seen from this picture.

In Figure 22 the second position of reinforcement is depicted together with obvious movement of the ridge. Also in the upper right part of the slope partial damage is highlighted and according to the assumed shape of the slip curve the safety margin is derived.

It appears that for upper position of the nail one nail bears 12.29 kg load, two nails 16.15 kg and the necessary number of nails for higher value of the load can be extrapolated. For the lower position (second case) of the nail, one nail bears only 7.12 kg, two nails 9.78 kg etc. The bearing capacity is considered for safety margin 1.3, as most of standards consider.

It is worth noting that this approach for the identification of appropriate structure of slopes with reinforcement by nails can be applied to various types of slopes, even in non-homogeneous mediums. For this case and the AIM see (Procházka, 1990).

5. CONCLUSIONS

Three examples of utilization of the coupled modelling method have been mentioned. Coupled modeling of behavior of structures (mutual comparison of experimental and numerical models) becomes very powerful tool for assessment and design. The results of the experimental model tests served to formulate constitution relations for numerical modelling. On the basis of experiment results, internal parameters for numerical models can be determined. The procedure may be considered as a special case of inverse analysis. An experimental modelling is limited by the fact that the results are valid only in the frame of conditions characterizing experiment. Therefore it is advantageous to combine the experimental modelling with numerical methods and utilize of their positive features, the flexibility and high performance of numerical solutions where the input parameters can be change very fast.

ACKNOWLEDGMENT

This paper was prepared under financial support of the Grant Agency of the Academy of Sciences of the Czech Republic GA AV ČR, grant project No. IAA 2119402, and partly was sponsored from CIDEAS.

REFERENCES

Cundall, P.A.: 1971, A computer model for simulation progressive large scale movements of blocky rock systems, Symposium of the international society of rock mechanics, 132–150.

Desai, C.S. (ed. H. Mulhaus): 1994, Constitutive modelling using the Disturbed State Concept, Chapter 8, Continuum Models for Materials with Microstructure, John Wiley & Sons, London, UK.

Dvorak, G.J. and Procházka, P.: 1996, Thick-walled composite cylinders with optimal fibre prestress, Composites, Part B, 27B, 643–649.

Dvorak, G.J.: 1992, Transformation Field Analysis of inelastic composite materials, Royal Society of London A 437, 311-327.

Jao, M. and Wang, M.C.: 2000, Behaviour of soft ground tunnel under strip footing, Trends in Rock Mechanics, Geotech. special publication, No. 102, ASCE, Denver, Colorado, 78–92.

Kachanov, L.M.: 1992, Introduction to Continuum Damage Mechanics, Martinus Nijhoff Publishers, Dordrecht, Netherlands.

Koudelka, P. and Procházka, P.: 2001, Apriori Integration method, analysis, similarity and optimization of slopes, Academia, Prague.

Kožešník, J.: 1983, Theory of similarity and modeling, Academia, Prague.

Moreau, J.J.: 1994, Some numerical methods in multibody dynamics: Application to granular materials, Eur. J. Mech. Solids, Vol.13, No.4, 93–114.

Procházka, J., Weiglová, K. and Trčková, J.: 2006, Coupled and comparative modelling of the underground structures, Brno, CERN.

Procházka, P. and Trčková, J.: 2000, Coupled modelling of concrete tunnel lining, Our World in Concrete and Structures, Singapore, 125–132.

Procházka, P. and Trčková, J.: 2001, Coupled modelling using DSC&TFA theoretical process, Proc. Computer methods and advances in geomechanics, Virginia, USA, A. A. Balkema, 389–394.

Procházka, P. and Válek, M.: 2000, Stability of Tunnel Face Using Coupled DSC & TFA Models, Damage and Fracture Mechanics VI. Montreal, WIT Press, 471–480.

Procházka, P. and Válek, M.: 2000, The BEM Formulation of Distinct Element Method, BETECH XXII. Cambridge: WIT Press, 395–404.

Procházka, P.: 1990, Slope optimization by the Apriori Integration Method, Acta Montana, IG CSAS, 82, 51–154.

Procházka, P.: 2003, Application of discrete element methods to fracture mechanics of rock bursts, Engng. Fract. Mech.

Trčková, J. and Procházka, P.: 2006, Stress changes around tunnel under the strip foundation. Proc. XIIIth Regional Rock Mechanical Symposium, Istambul, 15–22.

Trčková, J.: 2005, Study of stress changes around tunnel in dependence of the tunnel lining stiffness, Proc. 22th Danubia-Adria Symposium on Experimental Methods in Solid Mechanics, Monticelli Terme, 116–117.